Tectonophysics 619-620 (2014) 171–178

Contents lists available at ScienceDirect

Tectonophysics

journal homepage: www.elsevier.com/locate/tecto

Clay mineral anomalies in the Yingxiu–Beichuan fault zone from the WFSD-1 drilling core and its implication for the faulting mechanism during the 2008 Wenchuan earthquake (Mw 7.9)

Jialiang Si [a,b], Haibing Li [a,b,*], Liwei Kuo [c], Junling Pei [a,d], Shengrong Song [c], Huan Wang [a,b]

[a] State Key Laboratory of Continental Tectonics and Dynamics, Beijing, China
[b] Institute of Geology, Chinese Academy of Geological Sciences, Beijing, China
[c] Department of Geosciences, National Taiwan University, Taipei, China
[d] Institute of Geomechanics, Chinese Academy of Geological Sciences, Beijing, China

ARTICLE INFO

Article history:
Received 4 March 2013
Received in revised form 15 September 2013
Accepted 19 September 2013
Available online 26 September 2013

Keywords:
Yingxiu–Beichuan fault zone
Wenchuan earthquake
Clay minerals
Principal slip zone (PSZ)
WFSD-1

ABSTRACT

The first hole of the Wenchuan earthquake Fault Scientific Drilling (WFSD-1) was started on Nov. 6, 2008 as a rapid response to the May 12, 2008 Wenchuan earthquake (Mw 7.9), which slipped along the Longmen Shan fault on the eastern margin of the Tibetan Plateau. WFSD-1 was drilled to a depth of 1201.15 m and intersected the presumed active fault zone at a depth of 590 m (FZ590), which contains the maximum value of fracture density and fresh fault gouge. Here we characterized fault rocks of FZ590 by conducting XRD analyses with cohesive and non-cohesive rock samples collected from WFSD-1 borehole cores. The results indicate that a clay anomaly zone is located in the FZ590 fault zone. The slight enrichment of smectite distributed in fresh fault gouge implies that there is a fault-related authigenic clay formation. In addition, the location of the slight enrichment of smectite is consistent with the plausible active slip zone determined by previous results, adding confidence to the supposition that the principal slip zone (PSZ) of the 2008 Wenchuan earthquake is located at a depth of 589.2 m and situated at the lithological boundary of the Neoproterozoic Pengguan Complex and Triassic Xujiahe Formation. The tiny clay anomaly signal captured from borehole cores implies that low frictional heat was generated by coseismic slip, which drives only slight authigenesis processes. Thus, other dynamic weakening mechanisms, such as thermal pressurization may be involved in the fault zone of the Yingxiu–Beichuan fault during 2008 Wenchuan earthquake.

1. Introduction

The Mw 7.9 Wenchuan earthquake affected the whole country of China in 2008 and produced coseismic surface ruptures 270 km and 80 km long along the Yingxiu–Beichuan and Anxian–Guanxian faults, respectively (Fig. 1) (Fu et al., 2011; Li et al., 2008; Liu-Zeng et al., 2010; Xu et al., 2009). To obtain a better understanding of the mechanical, physical and chemical characteristics of the ruptured faults, the Wenchuan earthquake Fault Scientific Drilling project (WFSD) was undertaken with the support of Chinese government. The first borehole (WFSD-1), targeting the fault zone with the maximum co-seismic slip of the southern Yingxiu–Beichuan fault zone in Bajiaomiao Village, was drilled just 178 days after the earthquake where the surface vertical displacement was about 6 m (Li et al., 2008) (Fig. 1) and the horizontal displacement was about 3 m. WFSD-1 obtained 1201.15 m of core with a recovery rate of 95.4% and 12 fault zones were recognized in the core profile (Fig. 2).

Fault cores, accumulating the most slip and shear stress during an individual coseismic event, are often characterized by abundant clayey gouge (Caine et al., 1996). As the most common constituent of fault gouge, the characteristics of clay minerals may allow us to infer mechanical properties of the fault zone (Collettini et al., 2009a, 2009b; Moore and Lockner, 2008; Moore and Rymer, 2007; Saffer et al., 2001; Tembe et al., 2010), and physical-chemical processes taking place during coseismic and interseismic periods, such as the fluid-rock interaction, e.g., illite–smectite reaction (Solum et al., 2005; Vrolijk and Pluijm, 1999), and the pseudotachylyte–smectite transformation (Janssen et al., 2013; Kuo et al., 2009).

In the case of the Taiwan Chelungpu fault Drilling Project (TCDP), the location of the principal slip zone (PSZ: Sibson, 2003) was determined through physical, chemical, microstructural and seismological observations (Boullier et al., 2009; Boutareaud et al., 2008, 2010; Chou et al., 2012a,b; Hirono et al., 2006a,b, 2008; Ishikawa et al., 2008; Kuo et al., 2009, 2011, in press; Ma et al., 2006; Mishima et al., 2006, 2009). The characteristics of clay minerals within the TCDP PSZ suggest that frictional melting localized in a thickness of 1-mm took place and produced

* Corresponding author at: Institute of Geology, Chinese Academy of Geological Sciences, Beijing, China. Tel.: +86 10 68990581; fax: +86 10 68994781.
E-mail address: lihaibing06@163.com (H. Li).

0040-1951/$ – see front matter © 2013 Elsevier B.V. All rights reserved.
http://dx.doi.org/10.1016/j.tecto.2013.09.022

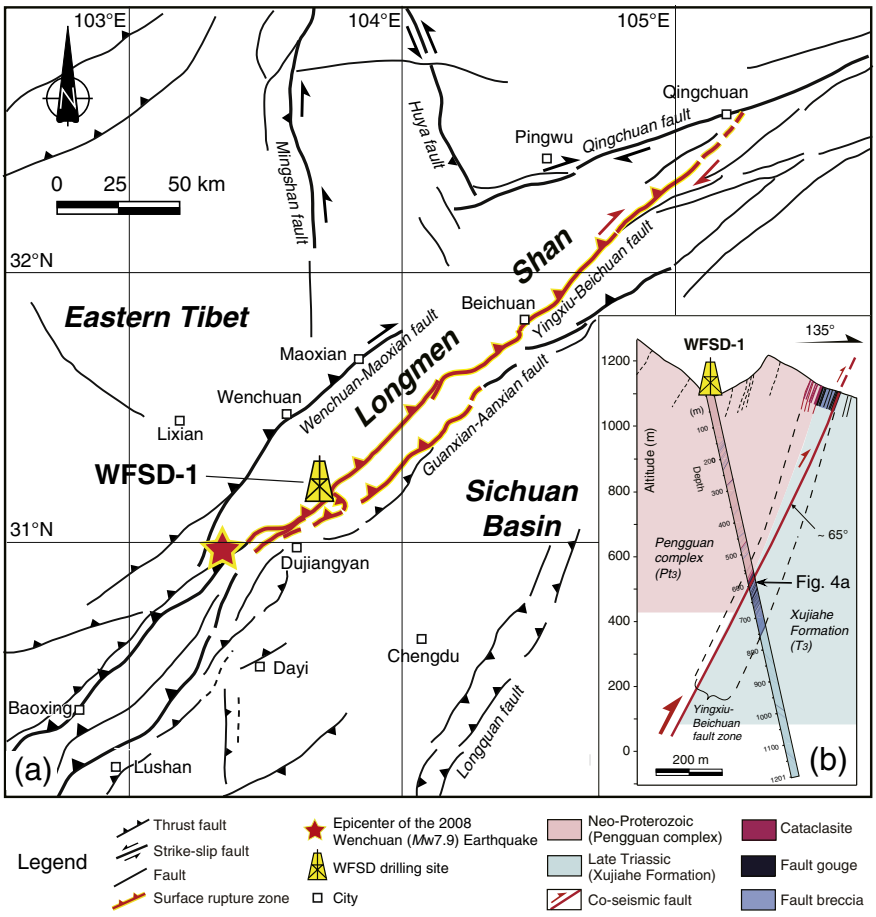

Fig. 1. Sketch map show the structures of the Longmen Shan, the adjacent area and the profile of the WFSD-1 borehole (revised after Li et al., 2013a). (a) Geological structures of the Longmen Shan and its adjacent area and WFSD drilling site location. (b) Geologic cross-section across the WFSD-1 site of the 1201 m hole. The Yingxiu–Beichuan fault zone is about 100 m wide in the WFSD-1 cores and with the dip angle of about 65° at a depth of ~1 km.

pseudotachylyte during the 1999 Chi-Chi earthquake, and that pseudotachylyte was transformed to smectite by the process of fluid infiltration (Kuo et al., 2009, 2011, in press).

Samples from drilled active faults, therefore, provide unique opportunities to determine in situ characteristics of fault rocks (e.g., Solum and Pluijm, 2004). WFSD-1 provides samples from depth, where the characteristics of clay minerals preserved within the active fault zone enable us to (1) determine the presumed location of the PSZ, (2) study the faulting behavior and (3) investigate the plausible faulting mechanism soon after a large earthquake. High gamma radiation, high porosity and P-wave velocity, as well as low resistivity and temperature anomalies indicate that the Wenchuan earthquake fault zone is located at 585.75–594.5 m-depth. Based on further examination of the core from the deep drilling project, the PSZ corresponding to the 2008 Wenchuan earthquake was suggested to be at a depth of 590 m (Li et al., 2013a,in this issue). To address the goals mentioned above, this paper will report the characteristics of clay minerals at depths surrounding 590 m, the analyses were performed on dense samples collected from borehole cores.

2. Tectonic setting

The Longmen Shan Mountains are the topographic boundary between the Tibetan Plateau and the Sichuan Basin with a steep topographic gradient and a high topographic relief of 3000–4500 m. As the front thrust belt of the Songpan–Ganzi orogen (Xu et al., 1992), the Longmen Shan fault zone is mainly composed of three thrust faults named the Wenchuan–Maoxian fault, the Yingxiu–Beichuan fault and the Guanxian–Anxian fault, from west to east (Fig. 1) (Li et al., 2006). In 2008, the Wenchuan earthquake (Mw 7.9) produced about 270 km and 80 km long surface ruptures along the NE-striking Yingxiu–Beichuan fault and Guanxian–Anxian fault, respectively (Fig. 1) (Li et al., 2008). The rupture zones generally followed those preexisting fault traces.

Based on detailed field work, the first hole of the Wenchuan earthquake Fault Scientific Drilling (WFSD-1) was sited at Bajiaomiao Village of Hongkou Town (Dujiangyan, Sichuan) (N31.149°, E103.691°) where the maximum vertical offset along the south segment of the Yingxiu–Beichuan fault developed (Fig. 1). The borehole is about 385 m west of the surface rupture, where Pengguan complex rocks outcrop in the hanging wall of the Yingxiu–Beichuan fault zone. This complex mainly consists of biotite granite, plagiogranite, mylonite, granodiorite, tonalite, intermediate-acidic intrusive rocks similar to diorite, and some mafic–ultramafic intrusive rocks, volcanics, pyroclastic rocks and metamorphic rocks of green schist phases (Li et al., 2013a). To intersect the Wenchuan earthquake fault zone at the shallowest possible depth, as well as study the characteristics of the fault zone and monitor the friction heat produced during the earthquake and its aftershocks, WFSD-1 was designed to be an inclined hole, with 80° inclination angle in the NE134° direction, i.e. perpendicular to the surface rupture zone whose strike was about ~NE40° (Fig. 1c) (Li et al., 2012). Due to a fracture of the 127 mm-wide casing, which occurred at 167 m-depth, a second hole from 166.88 m-depth had to be initiated. Another casing fracture occurred at 585 m and a third hole was sidetracked from 580 m. After

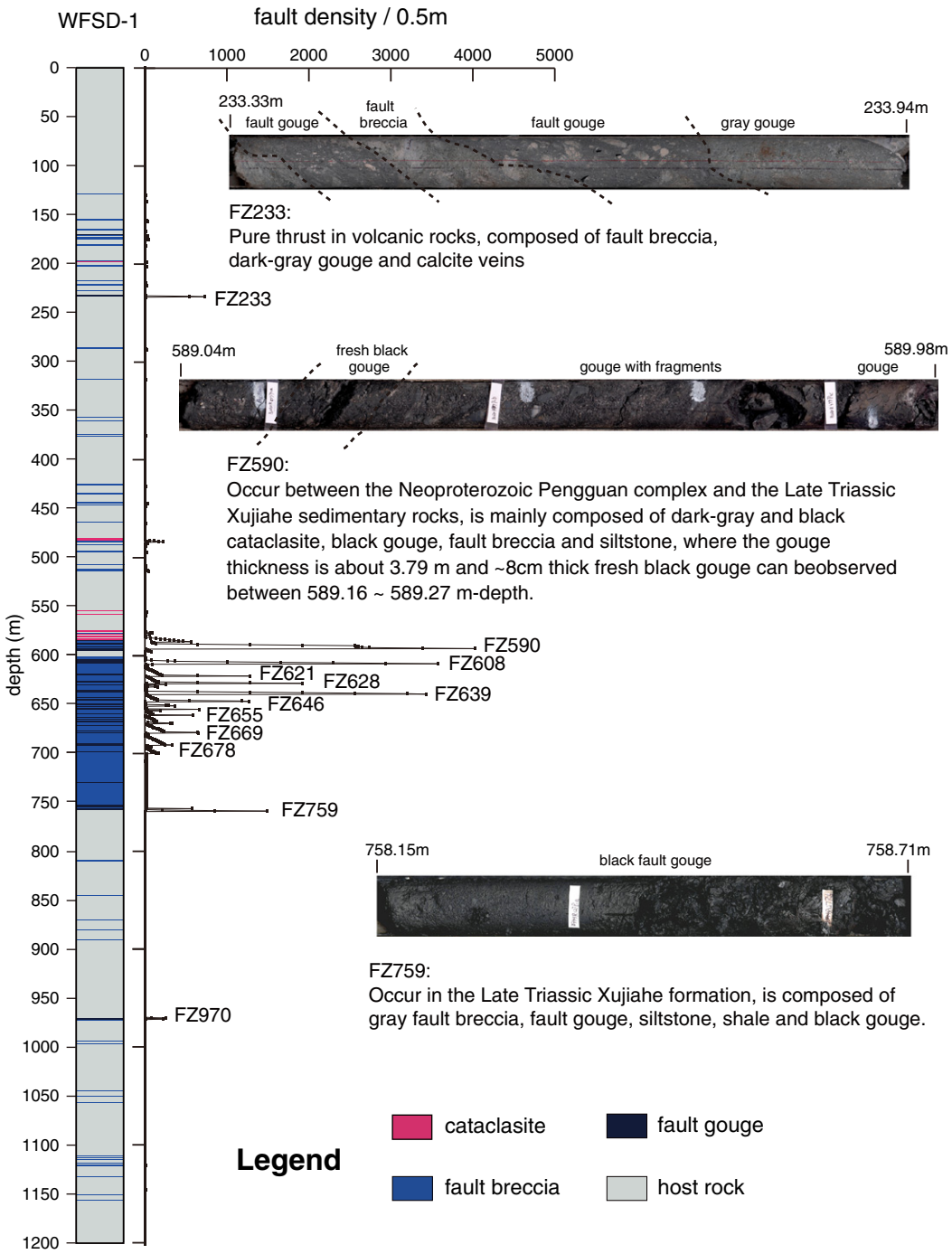

Fig. 2. Fault zone distribution in the WFSD-1 core and brief description of FZ233, FZ590 and FZ759. The left chart indicates the distribution of fault rocks. For specific calculation see Li et al. (2013a).

overcoming a variety of difficulties, the WFSD-1 borehole reached a depth of 1201.15 m, with a total core length of 1368.29 m (total core recovery rate was 95.4%) on July 12, 2009 (Li et al., 2013a).

In the WFSD-1 cores, 12 major fault zones were identified in the interval from 30 m to 1201 m and named after the depth as FZ233, FZ590, FZ608, FZ621, FZ628, FZ639, FZ646, FZ655, FZ669, FZ678, FZ759 and FZ970, with widths ranging from 1.8 m to 14.28 m and different gouge thicknesses (from 0.72 m to 3.79 m with the thickest gouge encountered in FZ590) (Fig. 2). The named depths of the fault zones correspond to the maximum fracture density which are generally in the middle of the gouge zones. Most fault zones have cumulative thick gouge layers composed of numerous sub-faults with thin gouge layers (such as FZ590 and FZ608). Three fault zones including FZ233, FZ590 and FZ759 are composed of a particularly large number of such sub-faults which might suggest an intense and long-term activation. The three fault zones (Fig. 2) are located in the Pengguan complex (FZ233), the Late Triassic Xujiahe Formation (FZ759) and the boundary zone between these two units (FZ590). The Xujiahe Formation is composed of sandstone, siltstone, shale and liquefied breccia.

3. Samples and analytical method

The WFSD-1 hole was drilled through the boundary of the upper Neoproterozoic Pengguan complex and the Triassic Xujiahe Formation

sedimentary rocks at a depth of 585.75 m. The borehole cores contained rock types such as diorite, volcanic rocks, pyroclastics, sandstone (including coal-bearing sandstone), siltstone, shale, liquefied breccias which result from soft sediment deformation (Qiao et al., 2012) and a series of fault-related rocks. In this study we collected 139 samples within the boundary of the Pengguan complex and Xujiahe Formation from depths of 584.68 m to 595.74 (FZ590 hereafter) to target the plausible active fault zone suggested by Li et al. (2013b).

X-ray Diffraction (XRD) analyses were conducted with a PANalytical X'Pert PRO X-ray diffractometer in National Taiwan University under the condition of filtered CuKα (1.540 Å) radiation at 45 kV and 40 mA, 1.0° min^{-1} scanning speed, and 5°–40° of 2θ interval for all analyses. Grain mounts of oriented clay samples were made for identifying and quantifying bulk rocks and clay minerals of <2 μm grainsize. For analyses of clay minerals, samples were disaggregated in distilled water using an ultrasonic bath. After centrifugation, suspensions of <2 μm fraction were deposited on glass slides. Two XRD runs were performed following air-drying and ethylene-glycol solvation for 72 h, to identify swelling clays (e.g., smectite). Identification of clay minerals was made mainly according to the position of the (001) series of the basal reflections on the air-dried and glycolated XRD diagrams. We utilize the most common approach for semi-quantitative analysis of clay minerals in powders, involving peak intensity ratios and mineral intensity factors (MIFs) (Kahle et al., 2002). This approach simplifies the general relationship between the integrated intensity of a diffraction peak area and the weight fraction of the mineral in a mixture. Peak areas of illite (10 Å), kaolinite (7 Å), and chlorite (14 Å) were divided based on their reflection factors, which were calculated on the glycolated curve. The mixed-layer phase of illite/smectite 001/001 (x > 10 Å) upon glycolation was determined (Biscaye, 1965; Fagel et al., 2003; Solum et al., 2003). Relative proportions of kaolinite and chlorite were determined on the basis of the ratio at the 3.57/3.54 Å peak area (Liu et al., 2007).

4. Results

The major mineral assemblages within the samples surrounding and within FZ590 via XRD analyses were identified as quartz, feldspar, and phyllosilicate minerals such as illite, smectite, chlorite, and kaolinite (Fig. 3). The variation of quartz, feldspar, illite, chlorite, and kaolinite within the samples surrounding and within FZ590 represents the normal variability of mineral proportion without significant anomalies of minerals. However, the relative proportion of smectite increases from 2% to 4% (Fig. 3). The XRD results of 1-cm interval sampling from a depth of 589.04 m to a depth of 589.53 m (50 samples) (Fig. 4a) show that the relative abundances of illite, chlorite and kaolinite have small variance (Table 1). Smectite is slightly enriched and its relative percentage increases from ~3 to 4 relative weight % at a depth of 589.22 m (Fig. 4b), which was the location of the plausible PSZ suggested by Li et al. (2013a) (Fig. 4c). In addition, the relative percentage of chlorite and kaolinite are slightly higher than the normal range, at 6% and 4%, respectively, in the depth range 589.38 m–589.39 m, and the relative percentage of quartz decreases to 30%. Overall, quartz and illite are the most abundant phases among the minerals, with an average abundance of 19–64% and 29–55%, respectively. Chlorite and kaolinite are less abundant with an average content of 0–6% and 0–2%, respectively. The relative percentage of feldspar averages at 0–5%, except for the sample at a depth of 584.44 m (17%) which contains feldspar detrital material. Smectite is the least abundant clay mineral, with an average percentage ranging from 1 to 2%.

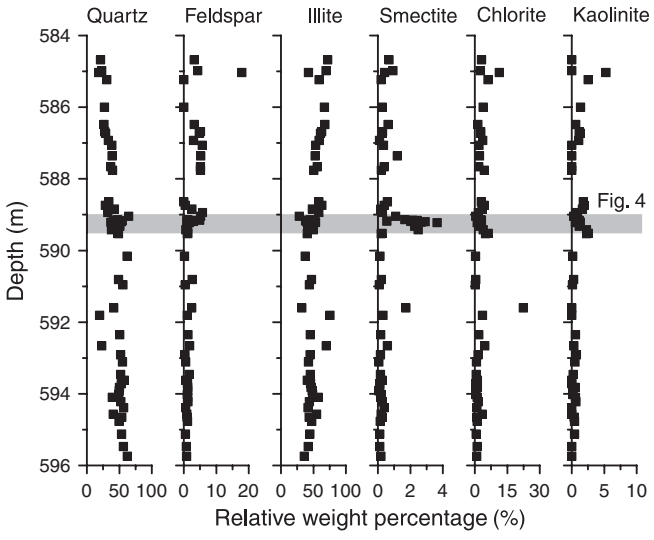

Fig. 3. Plot of relative weight percentage of major minerals and clay minerals from WFSD-1 cores from 584 m to 596 m in depth. The gray area shows the analyzed segment in Fig. 4.

The XRD patterns of 9 samples from a depth of 589.17 m to 589.25 m display a slight enrichment of smectite in the PSZ (Fig. 5a). In contrast, the XRD patterns of 7 samples from a depth of 589.35 m to 589.41 m show that the abundance of clay minerals remains similar in each sample for this interval (Fig. 5a). It is notable that very little graphite was detected in the XRD patterns at a depth of 589.2 m.

Swelling clays in our samples were determined through the XRD analysis under air-dried and glycolated conditions. The results suggest that smectite-rich illite phases were dominant (Fig. 5b). Here we follow the definition for illite provided by Meunier et al. (2004) and hereafter simply call a smectite-rich illite mixed-layer as smectite.

5. Discussion

5.1. Mineralogical changes in the fault gouges generated by coseismic faulting

The depth (~590 m) of the active fault zone in WFSD-1 corresponding to the 2008 Wenchuan earthquake was previously determined with conventional logging curves and temperature measurements (Li et al., 2012, 2013b). The darkest gouge layer can only be seen at the 8 cm-thick interval in FZ590 (589.17–589.25 m), which also has the highest magnetic susceptibility (Li et al., 2013a). In addition, continuous thin sections from the 589.04–589.34 m segment of WFSD-1 were made to check the microstructures. Several features that form by fault-related processes, such as calcite clasts and small veins, S-C fabrics and asymmetric rotational structures, were found in all thin sections. Within this interval, the thin section at a depth of 589.21–589.22 m contained an ultra-fine, uniform and clean matrix (Fig. 4c) and was suggested as the PSZ of the Yingxiu–Beichuan fault (Li et al., 2013a). It is reasonable to conclude that the signature of the in-situ physical-chemical processes (e.g., melting, dehydration, etc.) triggered by frictional heat during seismic slip might be recorded in the PSZ (e.g., Kuo et al., 2012).

In the TCDP case, significant variations were observed in the clay mineralogy within the 1 mm-thick PSZ of the Chelungpu fault and smectite was enriched by 80% (the abundance of smectite is none to rare in the host rock; Kuo et al., 2009, 2011, in press). The presumed mechanism for the clay anomaly formation in the TCDP borehole is that clay minerals that include illite, chlorite and kaolinite were thermally decomposed/dehydroxylated by frictional heat generated by coseismic slip, and then the products of the thermal decomposition/dehydroxylation processes (amorphous materials or pseudotachylyte) were altered into smectite (Kuo et al., 2009). Within the active Nojma fault zone, a similar transformation of glass-smectite was determined by TEM analysis and inferred the alteration of pseudotachylyte (Janssen et al., 2013). Thus, compared with the content of host rocks, the presence and/or the enrichment of smectite within the active fault

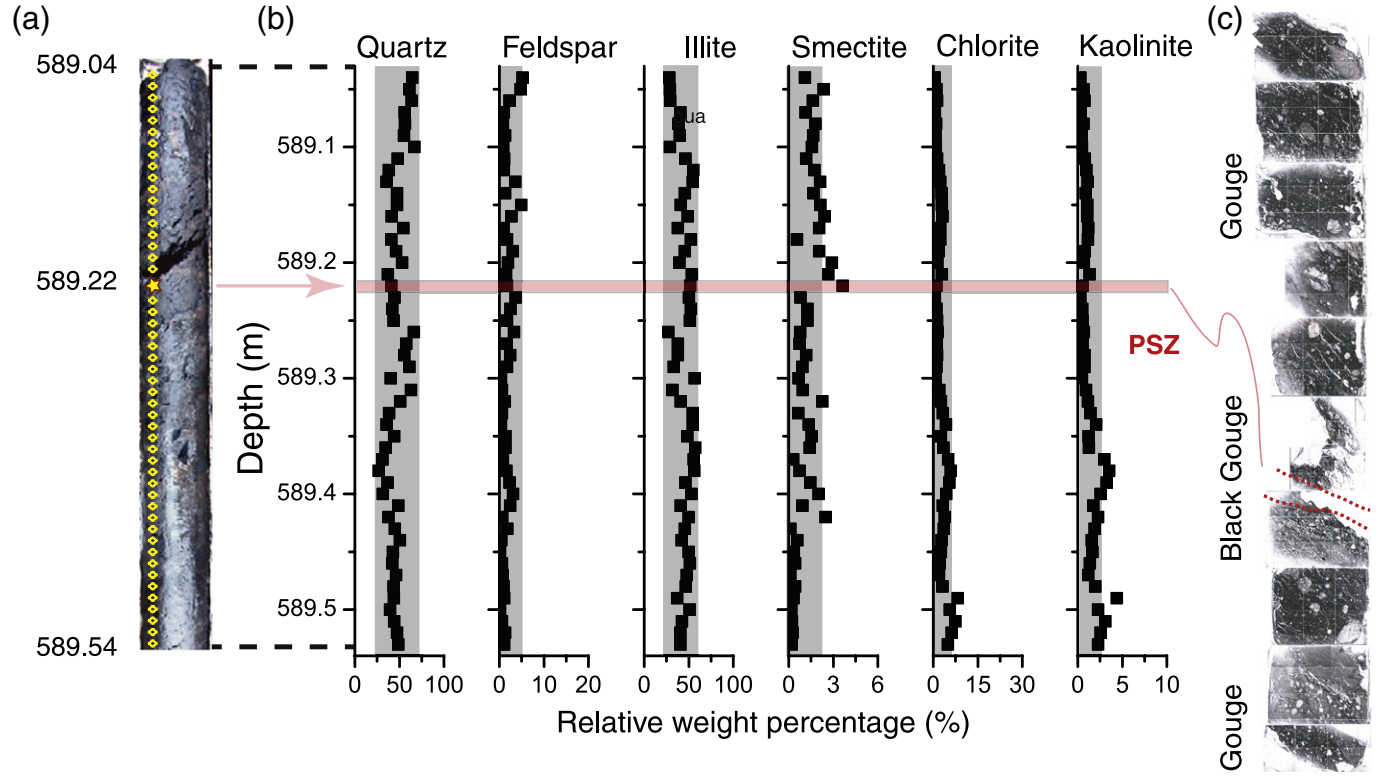

Fig. 4. (a) Image of black gouge analyzed with 1 cm intervals from 589.04 m to 589.54 m where the sampling locations are indicated by yellow. The sampling locations are indicated with red rhombus and pentagon symbols. (b) Detailed distribution of major minerals and clay minerals percentage across the FZ590. (c) Images of microstructures within the PSZ.

zones might be one piece of the evidence to identify the plausible PSZ during coseismic events.

In our study, a slight enrichment of smectite was discovered within the FZ590 PSZ which was suggested by Li et al. (2013a) to have slipped during the 2008 Wenchuan earthquake (Fig. 5a). Several mechanisms could be responsible for the formation of smectite within the PSZ such as (1) deposition by sedimentary processes, (2) illite/smectite reaction, and (3) glass/smectite transformation (Kuo et al., 2009; Solum et al., 2005; Velde et al., 1986; Vrolijk and Pluijm, 1999). The deposition by sedimentary processes might play a role, but can only supply a very small amount of smectite, since the abundance of smectite in all analyzed samples is shown to be less than 2%. Enrichment of smectite within the PSZ might be the result of fault-related processes of the illite/smectite reaction and glass/smectite transformation (Kuo et al., 2009; Solum et al., 2005).

The XRD patterns of air-dried and glycolated condition samples indicate that smectite was present in all samples and was more abundant within the PSZ (Fig. 5b). Smectite is classified by the number and degree of ordering of smectite- and illite-like interlayers. The degree of ordering is expressed by 'Reichweite' (R), where R0 corresponds to random interlayering, R1 corresponds to alternating illite and smectite interlayers, R2 corresponds to two smectite interlayers followed by an illite, etc. The number of interlayers given by the percent smectite seems to be different between the samples of the PSZ and the sample within the FZ590 (Fig. 5b), but the exact interlayers of smectite and illite could not be identified in our study. Further work, such as XRD patterns for various mixtures of illite and illite–smectite (with varying numbers and orderings of smectite interlayers) are required to reference our results and the TEM analyses. However, the additional abundance of smectite within the PSZ is likely the result from fault-related authigenesis (e.g., illite/smectite reaction and/or pseudotachylyte/smectite transformation) (Kuo et al., 2009; Solum et al., 2005).

Another anomaly of clay minerals within FZ590 was the slightly increased abundance of chlorite and kaolinite and the slightly decreased quartz content at a depth of 589.4 m (Fig. 4). The similar XRD patterns of analyzed samples at this depth indicate that the ratio of chlorite and kaolinite in each sample is roughly equivalent. Thus, the increase of the abundance of chlorite and kaolinite might be the result of the high abundance of clay minerals, which causes the decrease in the abundance of quartz.

5.2. The implication for the faulting mechanism

The strength of seismogenic faults in terms of frictional resistance has been a major subject of debate in fault mechanics for several decades (Collettini et al., 2009a, 2009b; Scholz, 2002; Zoback et al., 1987). Several slip weakening mechanisms have been suggested in the literature to account for low frictional strength of faults during earthquake propagation: flash heating (Rice, 2006), thermal pressurization (Rice, 2006; Sibson, 1973), frictional melting (Di Toro et al., 2006; Hirose and Shimamoto, 2005; Spray, 1987), gel formation (Di Toro et al., 2004; Goldsby and Tullis, 2002), thermal decomposition (Han et al., 2007), nanopowder lubrication (Han et al., 2010), recrystallization (Smith et al., 2012), graphitization (Oohashi et al., 2011), and elastohydrodynamic lubrication (Brodsky and Kanamori, 2001).

In the TCDP case, the Chi-Chi PSZ accommodated a coseismic displacement of 8.3 m (Ma et al., 2006), and the evidence of thermal perturbations (Chou et al., 2012a,b; Hirono et al., 2006b, 2008; Ishikawa et al., 2008; Kuo et al., 2009, 2011; Mishima et al., 2006, 2009) and fluid infiltrations (Boullier et al., 2009; Chou et al., 2012a,b; Ishikawa et al., 2008) within the PSZ were obtained from borehole core samples. Combined with the current data mentioned above, the faulting mechanism of the Chelungpu fault during 1999 Chi-Chi earthquake could be explained as melt lubrication and/or thermal pressurization.

Table 1
XRD test result of black gouge samples with 1-cm interval from 589.04 m to 589.54 m in depth.

Depth (m)	Quartz	Feldspar	Illite	Smectite	Chlorite	Kaolinite
589.04	64.35	5.22	28.13	1.09	0.42	0.27
589.05	61.33	4.74	28.93	2.35	1.06	0.64
589.06	63.62	2.25	29.33	1.62	1.27	0.76
589.07	55.77	1.02	40.68	1.14	0.52	0.33
589.08	56.25	0.81	38.29	1.79	0.97	0.64
589.09	55.24	1.26	40.01	1.65	0.7	0.43
589.1	67.01	0.82	28.67	1.56	0.83	0.48
589.11	48.09	1.06	46.28	1.18	1.25	0.79
589.12	38.16	1.02	55.2	1.72	1.95	0.97
589.13	35.55	3.53	54.39	2.11	2.3	1.1
589.14	47.47	1.31	45.48	1.66	2.79	0.88
589.15	47.41	4.91	40.95	2.13	2.92	1.07
589.16	41.33	2.67	48.83	2.42	3.09	1.08
589.17	54.5	0.95	37.81	2.06	2.34	1.17
589.18	40.75	1.72	52.35	0.56	2.38	1.15
589.19	46.14	3	45.62	2.04	1.81	0.79
589.2	53.05	1.91	39.38	2.9	1.38	0.69
589.21	37.07	1.48	53.52	2.66	2.87	1.31
589.22	40.83	1.7	51.74	3.64	1.11	0.52
589.23	44.41	3.6	50.07	0.8	0.58	0.28
589.24	42.03	2.46	52.22	1.27	1.12	0.5
589.25	43.56	1.68	51.29	1.26	1.27	0.54
589.26	66.19	3.3	27.01	0.77	1.46	0.68
589.27	57.7	1.66	37.72	0.72	1.14	0.55
589.28	55.62	2.4	37.7	1.18	1.24	0.74
589.29	61.09	1.69	32.94	0.92	1.12	0.75
589.3	40.31	0.37	56.69	0.66	0.79	0.47
589.31	63.04	0.59	31.73	0.93	2.06	0.92
589.32	51.06	1.2	40.9	2.27	2.53	1.13
589.33	38.48	0.6	54.48	0.65	3.2	1.43
589.34	35.52	0.33	54.59	1.34	4.26	2.05
589.35	43.96	1.35	48.25	1.54	2.53	1.22
589.36	34.56	1.38	57.27	1.4	3.37	1.26
589.37	30.92	0.78	55.58	0.29	4.97	2.98
589.38	26.62	1.59	56.37	0.73	5.88	3.53
589.39	36.53	2.26	46.34	1.45	5.47	3.24
589.4	31.28	3.06	53.04	2	4.33	2.56
589.41	48.74	2.44	40.8	0.91	3.16	1.76
589.42	37.6	0.63	49.95	2.48	3.89	2.27
589.43	44.96	1.78	45.6	0.11	3.53	1.88
589.44	50.48	0.43	42.06	0.58	2.76	1.58
589.45	42.82	0.15	49.72	0.34	2.61	1.63
589.46	42.13	0.56	51.07	0.43	2.18	1.36
589.47	46.44	0.68	47.74	0.11	1.89	1.18
589.48	43.51	0.93	46.78	0.42	3.13	1.96
589.49	43.86	1.05	37.14	0.33	8.26	4.39
589.5	39.36	0.14	50.9	0.17	5.5	2.29
589.51	44.1	0.54	42.38	0.22	7.48	3.09
589.52	47.26	1.31	40.68	0.26	6.15	2.55
589.53	48.87	1.08	40.69	0.2	4.88	2.28

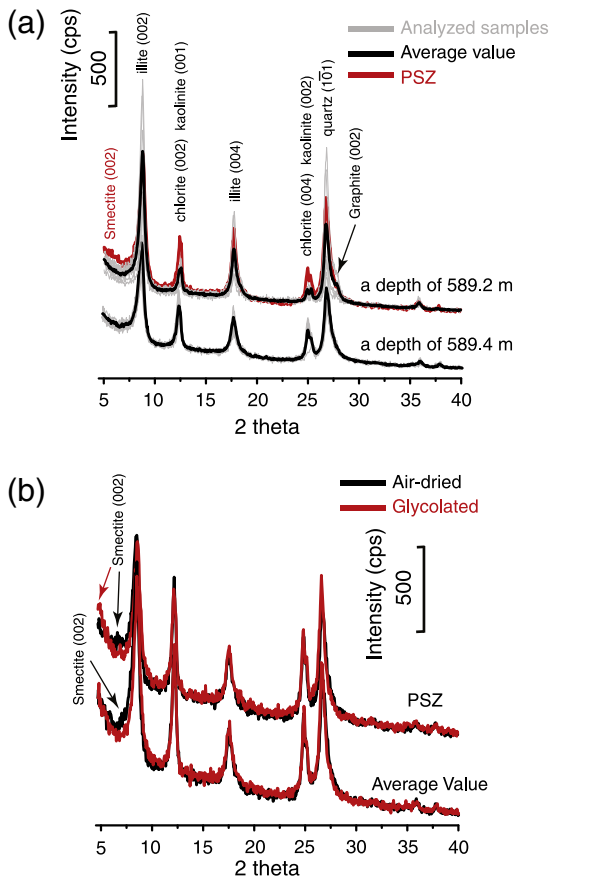

Fig. 5. (a) The clay mineral assemblage is quantified using X-ray diffraction patterns with the samples at a depth of 589.2 and 589.4 m. All XRD results are shown with gray lines, and the average value of all experiments is shown in black. The results of the PSZ are shown in red. (b) X-ray diffraction patterns of PSZ and samples at a depth of 589.4 m under air-dried and glycoated condition were shown for the identification of the presence of smectite.

In our study, the Wenchuan PSZ accommodated a coseismic displacement of 6 m (Li et al., 2012) but only slight mineralogical changes to the PSZ were observed in the borehole cores. This suggests that total frictional heat generated during coseismic slip of several meters would be small. This finding is in agreement with preliminary temperature measurements performed less than one year after drilling, which resulted in the detection of a small thermal anomaly (<0.15 °C) in the vicinity of the natural PSZ (Brodsky et al., 2012; Mori et al., 2010). Thus, our results suggest that the coefficient of friction during seismic faulting was extremely low. We thus suggest that possible weakening mechanisms associated with low temperature, e.g., powder lubrication (Han et al., 2007; Reches and Lockner, 2010), flash heating (Goldsby and Tullis, 2011), and thermal and thermochemical pressurization (Rice, 2006; Brantut et al., 2010; Ferri et al., 2010), might be involved during the 2008 Wenchuan earthquake.

In addition, the Yingxiu–Beichuan fault zone is about 240 m-wide at the outcrop while it is about 100 m in the WFSD-1 drilling core. We can also find gouge veins at the outcrop that were injected into the fault breccia, which indicate fluidization from thermal pressurization during fault activity (Wang et al., 2013). Therefore, the dynamic weakening mechanisms can likely be assumed to be thermal pressurization during the 2008 Wenchuan earthquake.

6. Conclusion

We characterized the fault rocks within the FZ590 and suggest that it is the active fault zone corresponding to 2008 Wenchuan earthquake. Our results indicate that at a depth of 589.2 m there is a zone of anomalous clay abundance, within which the abundance of smectite was slightly enriched. The slight enrichment of smectite distributed in fresh fault gouge suggests that fault-related authigenesis processes took place during or after coseismic events. The location of slight enrichment of smectite is consistent with the plausible principal slip zone (PSZ) location determined with the current results. The tiny clay anomaly signal observed in the borehole cores implies that low frictional heat was generated by coseismic slips, and dynamic weakening mechanisms such as thermal pressurization may have lubricated the fault zone of the Yingxiu–Beichuan fault during 2008 Wenchuan earthquake.

Acknowledgments

This work was supported by the "Wenchuan Earthquake Fault Scientific Drilling" of the National Science and Technology Planning Project, the National Natural Science Foundation of China (41102135) and the China Geological Survey Project (1212011220264, 1212011121267). We thank the Wenchuan Earthquake Fault Scientific Drilling Centre staff for their

help; thank the field drilling and well logging people by the 403 geological survey team of the Sichuan Geology & Mineral Resources Bureau. We also thank the guest editor and two anonymous reviewers for their valuable comments and suggestions improving this manuscript.

References

Biscaye, P.E., 1965. Mineralogy and sedimentation of recent deep-sea clay in the Atlantic Ocean and adjacent seas and oceans. Geol. Soc. Am. Bull. 76, 803–832.

Boullier, A.M., Yeh, E.C., Boutareaud, S., Song, S.R., Tsai, C.H., 2009. Microscale anatomy of the 1999 Chi-Chi earthquake fault zone. Geochem. Geophys. Geosyst. 10 (3), Q03016. http://dx.doi.org/10.1029/2008GC002252.

Boutareaud, S., Calugaru, D.G., Han, R., Fabbri, O., Mizoguchi, K., Tsutsumi, A., Shimamoto, T., 2008. Clay-clast aggregates: a new textural evidence for seismic fault sliding? Geophys. Res. Lett. 35 (5).

Boutareaud, S., Boullier, A.M., Andréani, M., Calugaru, D.G., Beck, P., Song, S.R., Shimamoto, T., 2010. Clay clast aggregates in gouges: new textural evidence for seismic faulting. J. Geophys. Res. 115, B02408. http://dx.doi.org/10.1029/2008jb006254.

Brantut, N., Schubnel, A., Corvisier, J., Sarout, J., 2010. Thermochemical pressurization of faults during coseismic slip. J. Geophys. Res. 115, B05314. http://dx.doi.org/10.1029/2009JB006533.

Brodsky, E., Kanamori, E.H., 2001. Elastohydrodynamic lubrication of faults. J. Geophys. Res. 106, 16357–16374.

Brodsky, E.E., Li, H.B., Mori, J.J., Kano, Y., Xue, L., 2012. Frictional stress measured through temperature profiles in the Wenchuan scientific fault zone drilling project. Eos Trans. Amer. Geophys. Union 93 (51) (Fall Meeting Supplementary, Abstract T44B-07.).

Caine, J.S., Evans, J.P., Forster, C.B., 1996. Fault zone architecture and permeability structure. Geology 24, 1025–1028.

Chou, Y.M., Song, S.R., Aubourg, C., Lee, T.Q., Boullier, A.M., Song, Y.F., Yeh, E.C., Kuo, L.W., Wang, C.Y., 2012a. An earthquake slip zone is a magnetic recorder. Geology. http://dx.doi.org/10.1130/G32864.1.

Chou, Y.M., Song, S.R., Aubourg, C., Song, Y.F., Boullier, A.M., Lee, T.Q., Evans, M., 2012b. Pyrite alteration and neoformed magnetic minerals in the fault zone of the Chi-Chi earthquake (Mx 7.6, 1999): evidence for frictional heating and co-seismic fluids. Geochem. Geophys. Geosyst. 13 (8), Q08002. http://dx.doi.org/10.1029/2012GC004120.

Collettini, C., Niemeijer, A., Viti, C., Marone, C., 2009a. Fault zone fabric and fault weakness. Nature 462, 907–910. http://dx.doi.org/10.1038/nature08585.

Collettini, C., Niemeijer, A., Viti, C., Marone, C., 2009b. Fault zone fabric and fault weakness. Nature 462, 907–912.

Di Toro, G., Goldsby, D.L., Tullis, T.E., 2004. Friction falls towards zero in quartz rock as slip velocity approaches seismic rates. Nature 427, 436–439.

Di Toro, G., Hirose, T., Nielsen, S., Pennacchioni, G., Shimamoto, T., 2006. Natural and experimental evidence of melt lubrication of faults during earthquakes. Science 311, 647–649.

Ferri, F., Di Toro, G., Hirose, T., Shimamoto, T., 2010. Evidence of thermal pressurization in high-velocity friction experiments on smectite-rich gouges. Terra Nova 22, 347–353. http://dx.doi.org/10.1111/j.1365-3121.2010.00955.x.

Fagel, N., Boski, T., Likhoshway, L., Oberhaensli, H., 2003. Late Quaternary clay mineral record in Central Lake Baikal (Academician Ridge, Siberia). Paleogeography, Palaeoclimatology, Palaeoecology 193 (1), 159–179.

Fu, B.H., Shi, P.L., Guo, H.D., Okuyama, S., Ninomiya, Y., Wright, S., 2011. Surface deformation related to the 2008 Wenchuan earthquake, and mountain building of the Longmen Shan, eastern Tibetan Plateau. J. Asian Earth Sci. 40 (4), 805–824.

Goldsby, D.L., Tullis, T.E., 2002. Low frictional strength of quartz rocks at subseismic slip rates. Geophys. Res. Lett. 29 (17), 1844.

Goldsby, D.L., Tullis, T.E., 2011. Flash heating leads to low frictional strength of crustal rocks at earthquake slip rates. Science 334 (6053), 216–218. http://dx.doi.org/10.1126/science.1207902.

Han, R., Shimamoto, T., Hirose, T., Ree, J.-H., Ando, J., 2007. Ultralow friction of carbonate faults caused by thermal decomposition. Science 316, 878–881.

Han, R., Hirose, T., Shimamoto, T., 2010. Strong velocity weakening and powder lubrication of simulated carbonate faults at seismic slip rates. J. Geophys. Res. 115, B03412.

Hirono, T., Lin, W., Yeh, E.C., Soh, W., Hashimoto, Y., Sone, H., Matsubayashi, O., Aoike, K., Ito, H., Kinoshita, M., Murayama, M., Song, S.R., Ma, K.F., Hung, J.H., Wang, C.Y., Tsai, Y.B., 2006a. High magnetic susceptibility of fault gouge within Taiwan Chelungpu fault: nondestructive continuous measurements of physical and chemical properties in fault rocks recovered from Hole B, TCDP. Geophys. Res. Lett. 33, L15303. http://dx.doi.org/10.1029/2006GL026133.

Hirono, T., Ikehara, M., Otsuki, K., Mishima, T., Sakaguchi, M., Soh, W., Omori, M., Lin, W., Yeh, E.C., Tanikawa, W., Wang, C.Y., 2006b. Evidence of frictional melting within disk-shaped black materials discovered from the Taiwan Chelungpu fault system. Geophys. Res. Lett. 33, L19311. http://dx.doi.org/10.1029/2006GL027329.

Hirono, T., Fujimoto, K., Yokoyama, T., Hamada, Y., Tanikawa, W., Tadai, O., Mishima, T., Tanimizu, M., Lin, W., Soh, W., Song, S.R., 2008. Clay mineral reactions caused by frictional heating during an earthquake: an example from the Taiwan Chelungpu fault. Geophys. Res. Lett. 35, L16303. http://dx.doi.org/10.1029/2008GL034476.

Hirose, T., Shimamoto, T., 2005. Growth of molten zone as a mechanism of slip weakening of simulated faults in gabbro during frictional melting. J. Geophys. Res. 110, B05202. http://dx.doi.org/10.1029/2004JB003207.

Ishikawa, T., Tanimizu, M., Nagaishi, K., Matsuoka, J., Tadai, O., Sakaguchi, M., Hirono, T., Mishima, T., Tanikawa, W., Lin, W., Kikuta, H., Soh, W., Song, S.R., 2008. Coseismic fluid–rock interactions at high temperatures in the Chelungpu fault. Nat. Geosci. 1. http://dx.doi.org/10.1038/ngeo308.

Janssen, C., Wirth, R., Lin, A., Dresen, G., 2013. TEM microstructural analysis in a fault gouge sample of the Nojima fault zone, Japan. Tectonophysics 583, 101–104. http://dx.doi.org/10.1016/j.tecto.2012.10.020.

Kahle, M., Kleber, M., Jahn, R., 2002. Review of XRD-based quantitative analyses of clay minerals in soils: the suitability of mineral intensity factors. Geoderma 109, 191–205.

Kuo, L.W., Song, S.R., Yeh, E.C., Chen, H.F., 2009. Clay mineral anomalies in the fault zone of the Chelungpu Fault, Taiwan, and their implications. Geophys. Res. Lett. 36 (L18306). http://dx.doi.org/10.1029/2009GL039269.

Kuo, L.W., Song, S.R., Huang, L., Yeh, E.C., Chen, H.F., 2011. Temperature estimates of coseismic heating in clay-rich fault gouges, the Chelungpu fault zones, Taiwan. Tectonophysics 502 (3–4), 315–327.

Kuo, L.W., Song, S.R., Yeh, E.C., Chen, H.F., Si, J., 2012. Clay mineralogy and geochemistry investigations in the host rock of the Chelungpu fault, Taiwan: implication for faulting mechanism. J. Asian Earth Sci. 59, 208–218.

Kuo, L.W., Hsiao, H.C., Song, S.R., Sheu, H.S., Suppe, J., 2013. Coseismic thickness of principal slip zone from the Taiwan Chelungpu fault drilling project-A (TCDP-A) and correlated fracture energy. Tectonophysics. http://dx.doi.org/10.1016/j.tecto.2013.07.006 (in press).

Li, Y., Zhou, R.J., Densmore, A.L., Ellis, M.A., 2006. Geomorphic evidence for the late Cenozoic strike-slipping and thrusting in Longmen Mountain at the eastern margin of the Tibetan Plateau. Quat. Sci. 26 (1), 40–51 (in Chinese with English abstract).

Li, H.B., Fu, X.F., Van der Word, J., Si, J.L., Wang, Z.X., Hou, L.W., Qiu, Z.L., Li, N., Wu, F.Y., Xu, Z.Q., Tapponnier, P., 2008. Co-seisimic surface rupture and dextral-slip oblique thrusting of the Ms 8.0 Wenchuan earthquake. Acta Geol. Sin. 82 (12), 1623–1643 (in Chinese with English abstract).

Li, H.B., Xu, Z.Q., Si, J.L., Song, S.R., Sun, Z.M., Chevalier, M.-L., 2012. Wenchuan earthquake fault scientific drilling program (WFSD): overview and results. Eos Trans. Amer. Geophys. Union 93 (51) (Fall Meeting Supplementary, Abstract T44B-01).

Li, H.B., Wang, H., Xu, Z.Q., Si, J.L., Pei, J.L., Li, T.F., Huang, Y., Song, S.R., Kuo, L.W., Sun, Z.M., Chevalier, M.L., Liu, D.L., 2013a. Characteristics of the fault-related rocks, fault zones and the principal slip zone in the Wenchuan Earthquake Fault Scientific Drilling Project Hole-1 (WFSD-1). Tectonophysics 584, 23–42.

Li, H.B., Niu, Y.X., Kong, G.S., Huang, Y., Wang, H., Si, J.L., Sun, Z.M., Pei, J.L., Gong, Z., Chevalier, M.L., Liu, D.L., 2013. Structural and physical properties characterization in the Wenchuan earthquake Fault Scientific Drilling project-hole 1 (WFSD-1). Tectonophysics. http://dx.doi.org/10.1016/j.tecto.2013.08.022 (in this issue).

Liu, Z., Colin, C., Huang, W., Le, K.P., Tong, S., Chen, Z., Trentesaux, A., 2007. Climatic and tectonic controls on weathering in South China and the Indochina Peninsula: clay mineralogical and geochemical investigations from the Pearl, Red, and Mekong drainage basins. Geochem. Geophys. Geosyst. 8, Q05005. http://dx.doi.org/10.1029/2006GC001490.

Liu-Zeng, J., Wen, L., Sun, J., Zhang, Z.H., Hu, G.Y., Xing, X.C., Zeng, L.S., Xu, Q., 2010. Surficial slip and rupture geometry on the Beichuan Fault near Hongkou during the Mw 7.9 Wenchuan Earthquake, China. Bull. Seismol. Soc. Am. 100 (5B), 2615–2650.

Ma, K.F., Tanaka, H., Song, S.R., Wang, C.Y., Hung, J.H., Tsai, Y.B., Mori, J., Song, Y.F., Yeh, E.C., Soh, W., Sone, H., Kuo, L.W., Wu, H.Y., 2006. Slip zone and energetics of a large earthquake from the Taiwan Chelungpu-fault Drilling Project. Nature 444, 473–476.

Meunier, A., Velde, B., Zalba, P., 2004. Illite K-Ar dating and crystal growth processes in diagenetic environments: a critical review. Terra Nova 16, 296–304. http://dx.doi.org/10.1111/j.1365-3121.2004.00563.x.

Mishima, T., Hirono, T., Soh, W., Song, S.R., 2006. Thermal history estimation of the Taiwan Chelungpu fault using rock-magnetic methods. Geophys. Res. Lett. 33.

Mishima, T., Hirono, T., Nakamura, N., Tanikawa, W., Soh, W., Song, S.R., 2009. Changes to magnetic minerals caused by frictional heating during the 1999 Taiwan Chi-Chi earthquake. Earth Planet. Space Lett. 61, 797–801.

Moore, D.E., Lockner, D.A., 2008. The friction in the temperature range 25°–400 °C: relevance for fault-one weakening. Tectonophysics 449, 120–132.

Moore, D.E., Rymer, M.J., 2007. Talc-bearing serpentinite and the creeping section of the San Andreas fault. Nature 448, 795–797.

Mori, J., Li, H., Wang, H., Kano, Y., Pei, J., Xu, Z., Brodsky, E., 2010. Temperature measurements in the WFSD-1 borehole following the 2008 Wenchuan earthquake (Mw7.9). Eos Trans. Amer. Geophys. Union 91 (51) (Fall Meeting Supplementary, Abstract T53E-03.).

Oohashi, K., Hirose, T., Shimamoto, T., 2011. Shear-induced graphitization of carbonaceous materials during seismic fault motion: experiments and possible implications fault mechanics. J. Struct. Geol. 33, 1122–1134.

Qiao, X.F., Guo, X.P., Li, H.B., Gou, Z.H., Su, D.C., Tang, Z.M., Zhang, W., Yang, G., 2012. Soft-sediment deformation in the Late Triassic and the Indosinian tectonic movement in Longmen Shan. Acta Geol. Sin. 86 (1), 132–156.

Reches, Z., Lockner, D.A., 2010. Fault weakening and earthquake instability by powder lubrication. Nature 467 (7314), 452–455. http://dx.doi.org/10.1038/nature09348.

Rice, J.R., 2006. Heating and weakening of faults during earthquake slip. J. Geophys. Res. 111, B05311.

Saffer, D.M., Frye, K., Marone, C., Mair, K., 2001. Laboratory results indicating weak and potentially unstable frictional behavior of smectite clay. Geophys. Res. Lett. 28. http://dx.doi.org/10.1029/2001GL012869.

Scholz, C.H., 2002. The Mechanics of Earthquakes and Faulting. Cambridge Univ. Press.

Sibson, R.H., 1973. Interactions between temperature and pore fluid pressure during earthquake faulting: a mechanism for partial or total stress relief. Nature 243, 66–68.

Sibson, R.H., 2003. Thickness of the seismic slip zone. Bull. Seismol. Soc. Am. 93 (3), 1169–1178.

Smith, S.A.F., Di Toro, G., Kim, S., Ree, J.H., Nielsen, S., Billi, A., Spiess, R., 2012. Coseismic recrystallization during shallow earthquake slip. Geology. http://dx.doi.org/10.1130/G33588.1.

Solum, J.G., Pluijm, B.A., 2004. Phyllosilicate mineral assemblages of the SOFAD pilot hole and comparison with an exhumed segment of the San Andreas fault system. Geophys. Res. Lett. 31, L15S19. http://dx.doi.org/10.1029/2004GL019909.

Solum, J.G., Pluijm, B.A., Peacor, D.R., 2005. Neocrystallization, fabrics and age of clay minerals from an exposure of the Moab Fault, Utah. J. Struct. Geol. 27, 1563–1576.
Spray, J.G., 1987. Artificial generation of pseudotachylite using friction welding apparatus: simulation of melting on a fault plane. J. Struct. Geol. 9, 49–60.
Tembe, S., Lockner, D.A., Wong, T.F., 2010. Effects of clay content and mineralogy on frictional sliding behavior of simulated gouges: binary and ternary mixtures of quartz, illite, and montmorillonite. J. Geophys. Res. 115, B03416.
Velde, B., Suzuki, T., Nicot, E., 1986. Pressure–temperature-composition of illite/smectite mixed-layer minerals: Niger delta mudstones and other examples. Clays Clay Miner. 34 (4), 435–441.
Vrolijk, P., Pluijm, B.A., 1999. Clay gouge. J. Struct. Geol. 21, 1039–1048.
Wang, H., Li, H.B., Si, J.L., Sun, Z.M., Huang, Y., 2013. Internal structure of the Wenchuan earthquake fault zone, revealed by surface outcrop and WFSD-1 drilling core investigation. Tectonophysics. http://dx.doi.org/10.1016/j.tecto.2013.08.029.
Xu, Z.Q., et al., 1992. Orogenic Processes of the Songpan Ganze Orogenic Belt of China. Geological Press, Beijing 1–190 (in Chinese).
Xu, X.W., Wen, X.Z., Yu, G.H., Chen, G.H., Klinger, Y., Hubbard, J., Shaw, J.H., 2009. Coseismic reverse- and oblique-slip surface faulting generated by the 2008 Mw 7.9 Wenchuan earthquake, China. Geology 37 (6), 515–518.
Zoback, M.D., Zoback, M.L., Mount, V.S., Suppe, J., Eaton, J.P., Healy, J.H., Oppenheimer, D., Reasenberg, P., Jones, L., Raleigh, B., Wong, I.G., Scotti, O., Wentworth, C., 1987. New evidence on the state of stress of the San Andreas fault system. Science 238, 1105–1111.